

Deep Learning and Gaussian Process based Band Assignment in Dual Band Systems

Daoud Burghal, *Student Member, IEEE*, Rui Wang, *Student Member, IEEE*, and
Andreas F. Molisch *Fellow, IEEE*

Abstract

We consider the band assignment (BA) problem in dual-band systems, where the basestation (BS) chooses one of the two available frequency bands (centimeter-wave and millimeter-wave bands) to communicate with the user equipment (UE). While the millimeter-wave band might offer higher data rate, there is a significant probability of outage during which the communication should be carried on the (more reliable) centimeter-wave band. We consider two variations of the BA problem, one-shot and sequential BA. For the former the BS uses only the currently observed information to decide whether to switch to the other frequency band, for the sequential BA, the BS uses a window of previously observed information to predict the best band for a future time step. We provide two approaches to solve the BA problem, (i) a deep learning approach that is based on Long Short Term Memory and/or multi-layer Neural Networks, and (ii) a Gaussian Process based approach, which relies on the assumption that the channel states are jointly Gaussian. We compare the achieved performances to several benchmarks in two environments: (i) a stochastic environment, and (ii) microcellular outdoor channels obtained by ray-tracing. In general, the deep learning solution shows superior performance in both environments.

Index Terms

Machine Learning, Side Information, Dual Mode base-station, Frequency Band Switching.

I. INTRODUCTION

The large available bandwidths in the millimeter-wave (mmWave) frequency band can support the high data rates required for many emerging applications in next generation wireless networks (5G and beyond). However, the hostile propagation conditions at high frequencies restrict its

This work was supported financially in part by the National Science Foundation.

The authors are at the Ming Hsieh Department of Electrical Engineering, University of Southern California, Los Angeles, CA 90089, USA (email: burghal,wang78,molisch@usc.edu).

utilization. Compared to the centimeter-wave (cmWave) band,¹ signals in the mmWave band suffer from higher attenuation, higher diffraction loss, and are more susceptible to blockage, which reduces the reliability of the communication systems [1], [2], a required criterion for seamless user experience. Thus, due to these characteristics of the two bands, *both* are indispensable components for future wireless networks [3], [4]. The *joint* utilization of the two bands enhances the coverage, system reliability and achievable data rates.

Recently, different dual band architectures were proposed [4]–[6]. For instance, the cmWave band can be used for the control plane while the mmWave band is used for the data plane. Alternatively, both bands can be used for both planes. In some wireless networks, the *simultaneous* usage of the two bands might not be practical due to a number of limitations at the User Equipment (UE) side, such as limited processing capabilities, constraints on transmission power, etc. Thus, depending on the underlying band assignment (BA) scenario, the basestation (BS)² has to assign the UE to one of the two bands based on the instantaneously observed channels, such as in the initial channel access scenario, or sequentially switch the communication between the two bands as the UE moves, i.e., switch to the mmWave band whenever it is available or the cmWave band when the mmWave band suffers a blockage or other bad propagation conditions. We refer to the first problem as *one-shot* BA, and the second as *sequential* BA.

The BA problem is challenging, since simultaneous observations of the two bands are not usually available to the BS. Furthermore, using a frequent "measurement gap" to send training signals over the two bands and synchronizing such (possibly) unnecessary switching between the bands reduces the overall throughput of the system. In an alternative solution that relies on the correlation and the joint characteristics of the two bands, the BS can utilize partial information, such as the channel state in one band or the UE's location, together with some "prior knowledge" to solve the BA problem. Both the accurate joint characterizations of the two bands and the proper utilization of such (possibly) non-homogeneous information are also challenging. In this paper, we concentrate on the latter problem; for the former, see, e.g., [7] and references therein.

Machine learning (ML) is a powerful technique that can capture complex relations between the input data (features) and the output values (labels). Motivated by the remarkable success

¹In a slight abuse of notation, we call here the sub-6GHz band the cmWave band, and 24-100 GHz the mmWave band. This is inspired by the current 3GPP and WiFi frequency ranges.

²We use the term BS as a generic expression for the gNodeB in 3GPP New Radio, or an Access Point with both 802.11ac/ax and 802.11ad/ay in WiFi.

of Deep ML (DL) in various fields, the wireless communication community started recently to explore DL in problems such as channel coding, estimation, channel modeling and many others, see., e.g., [8]–[10] and references therein. The reported initial results are promising; ML based solutions are able to provide competitive performance for problems where optimal solutions are known, e.g., using multi-layer Neural Networks (NNs) for decoding in AWGN channel [11], indicating that ML may also be applied to problems where traditional methods have failed or where the environment is too complex. For instance, Ref. [12] demonstrated the efficiency of DL based detection over a molecular system where the channel model is difficult to model.

In this work we consider two different approaches to solving the BA scenarios. In the first approach, we use standard assumptions about the channel model to derive analytical solutions to the problem. In particular, we assume that the shadowing (on logarithmic scale) in the two bands follows a joint Gaussian distribution over frequency and space, i.e., it represents a Gaussian Process (GP); this assumption extends the widely used model of lognormal shadowing in a single frequency band [1]. The second approach is motivated by the above discussion on the complexity of the BA and the promising performance of the ML solutions. Thus, we explore different ML models for *several* feature combinations that may include some information about the channel properties and/or location of the UE. We study the approaches in two different environments. The first is a stochastic environment, where the channel realizations are generated in accordance with the GP assumption. The second is a more realistic environment where the channel states are obtained via ray-tracing. Both environments are needed for fair and informative comparisons, as in the first the GP-based solution is optimal for a statistical channel model, and the second represents a realization of a realistic environment.

A. Prior Work

In addition to the papers that discussed possible advantages and architectures of dual band systems, there have been recent studies that considered the *interplay* between cmWave and mmWave bands. Refs. [2], [13], [14] utilize the angular correlation in the two bands to provide a coarse estimate of the Angle of Arrival (AoA) at mmWaves based on the AoAs in the cmWave band, which can be used to reduce the beam-forming complexity at the mmWave band. Ref. [15] studied the covariance matrix translation between the two bands. For joint communication in the two bands, [14] proposes a two-queue model to assign data to each band such that delay is minimized and throughput is maximized. Ref. [16] considers the downlink resource allocation in

a network with a small cell BS, where the BS aims to assign the UE or services to the resources in the two bands.

The BA process can be viewed as a handover process between two co-located BSs with different frequencies. Refs. [17]–[19] used ML approaches to address the handover and switching between BSs that may use different frequency bands. In [18], the authors use ML to improve the success rate in the handover between two co-located cells in different bands, their implemented ML classifier uses the prior channel measurements and handover decisions within a temporal window to predict the success of the handover. Ref. [17] introduces an uplink (ULink)/downlink (DLink) decoupling concept where the central BS gathers measurements of the Rician K-factor and the DLink reference signal receive power for both bands, and trains a non-linear ML algorithm that is then applied to the cmWave band data to predict the target frequencies and BS that can be used for the ULink and DLink. Ref. [19] uses a gated recurrent NN to predict handover status at the next time slot given the beam-sequence, where the BS uses the sequence of previously used *beam-forming* vectors as input to the ML scheme. Different than these works we use different sets of features and several ML algorithms (including a DL solution based on recurrent NN) for two problem setups in two different environments, enabling us to optimize a solution approach, and not just check the performance of one particular algorithm. In addition we also consider an analytical solution based on GP for the BA problem, which may not only be of value in itself, but also allows to benchmark the ML solution.

Channel states prediction using GP or ML was considered in several works such as [20]–[23], where Refs. [20], [23] use GP to predict the shadowing values in the network based on collected drive tests, while Refs. [20]–[22] use regression ML techniques to predict the channel state. Using ML to predict unobserved channel features was also considered in [24], [25]; in [25] the authors use NNs to predict the AoA, and in [24] the authors utilize the observed channel state information in a central BS to predict the optimal beam direction in local BSs. However, these works focus on single band and use mainly a regression framework, while in this paper we solve the BA in two bands as a classification problem using several related features combination.

In our recent work [26] we derive the achievable rates and the outage probability of the BA based on linear prediction. In the current work, although using similar basic assumptions as [26] for the GP approach, the BA decisions are based on the probability of success. In addition, the ML part of this paper is a generalization to our previous conference paper [27], where here we include a sequential BA scenario.

B. Contribution

We consider GP-based and ML-based approaches to obtain solutions to two BA scenarios: one-shot and sequential BA. The one-shot scenario relies on the current observations for the BA, while the sequential BA the BS uses the current and previous observation to *predict* the best BA in a future time instant. The GP-based solution uses the GP assumption along with approximations, which may not always hold in practice, to derive analytically tractable solutions. In the ML based solution we use DL and other ML techniques to propose efficient solutions to the BA problems. The used observations depend on the scenario and the approach, which *may* include: the location of the UE, the received power (or data rate) in one band,³ the delay, and the Angle of Departure (AoD) of the main multi-path component (MPC) [1]. Utilizing such information, the BS can reduce the required signaling, which improves the spectrum efficiency and reduces the latency in the system. We study the performance of the proposed solutions in a ray-tracing and a stochastic environments, where the latter environment relies on the GP assumption to generate the shadowing. The contributions of this manuscript are threefold.

- We propose exact and approximate solutions to the BA based on the GP assumption, where we assume that the shadowing follows a GP in space and frequency; interestingly the approximate solution shows better results in channels where the GP does not hold.
- Viewing the BA as a classification problem, we use several ML approaches to solve the BA problem, which include linear regression (LR), Logistic Regression (GR), NNs, and DL based on Long Short Term Memory (LSTM) architectures. We use cross validation techniques to optimize their parameters. The use of several ML techniques is necessary to provide realistic assessment of the power of complex ML approaches.
- We study the performance of the proposed solutions under several features combinations in stochastic and ray-tracing environments. This is done because some of the features are available with little overhead, while others require significant acquisition effort.

The remainder of the paper is organized as follows. Sec. II describes the basic system model, summarizes the two problems, and introduces the two approaches along with their main assumptions. In Sec. III, we derive the BA rules under the GP assumption, and also provide an approximate solution. Sec. IV provides the details of the DL approach. Secs. V and VI provide

³We use the signal to noise ratio, signal strength and rate interchangeably when we refer to one of them as a feature, since we assume that we can use one of them to calculate the others, even though that might not be correct under some circumstances.

two experiments to evaluate the performance of the schemes, using a stochastic environment and a ray-tracing environment, respectively. Finally, Sec. VII provides concluding remarks.

II. PROBLEM AND SOLUTIONS OVERVIEW

A. Basic System Model

We consider a dual band cellular system, where the BS and the UE can operate in two frequency bands with center frequency f_b and bandwidth ω_b in band $b \in \{c, m\}$, where c and m refer to the cmWave and the mmWave bands, respectively. Due to a number of practical limitations of the UE, we assume that data transmission occurs in a single frequency band at a time. The BS controls the band selection process, using some observations about the channel and prior knowledge to choose the band that results in the highest data rate. To focus on the basic problem, we consider a single user case, i.e., no scheduling or interference is considered; the multi-user case is left for future work.

It is well established that the small scale fading in the two bands are independent due to the large frequency separation; furthermore, modern diversity techniques mostly eliminate its impact [1]. In contrast, large scale parameters vary relatively slowly over time and maintain time and frequency correlation, making it possible to utilize information over frequency and time (space) and thus make switching decisions. Note also that large-scale parameters are reciprocal in ULink and DLink for both time-domain and frequency-domain duplexing systems as long as the duplexing distance is smaller than the stationarity time or bandwidth, respectively; this condition is fulfilled for almost all practical systems. For this reason, the subsequent discussion is valid for both link directions, and we assume that the BS can acquire the channel state information about the large-scale parameters without additional overhead.

Similar to [26] we define a time-frame as a sequence of T time slots (data units), each time-frame is indexed with t . The SNR in band b on a logarithmic scale (dB) during time-frame t can be described by [1]

$$\text{SNR}^b(t) = P_{\text{tx}}^b + \zeta^b(t) - N_0^b, \quad (1)$$

where P_{tx}^b is the transmitted power (including both transmit and receive antenna gain), N_0^b is the noise level, and $\zeta^b(t)$ captures the large scale variation in band b that varies as the UE moves. Then using capacity-achieving transmission, we can write the rate in band b as

$$R^b(t) = \omega_b \log \left(1 + 10^{\gamma \text{SNR}^b(t)} \right). \quad (2)$$

where $\gamma = 0.1$. In this work, the BA procedure and the detailed description of the observations and prior knowledge depend on the scheme and the problem setup. In general, the BS uses the observations to produce the soft decision $\tilde{\mathcal{D}} \in [0, 1]$, which it then uses to make the BA decision $\mathcal{D} \in \{0, 1\}$, where we use "0" and "1" to refer to the data transmission in the cmWave and mmWave band, respectively.

B. Problem Description

We study two scenarios, other scenarios can be also considered, however, they generally lie between the two scenarios and/or can be derived based on the provided analysis, thus for brevity we do not discuss them here.

1) *One-Shot Band Assignment*: In this problem, for time-frame t , the BS uses the current observations to choose the frequency band for data communication, i.e., the observations, the BA decision and data transmission are all in the same time frame t . The used observations depend on the approach, but may include the observed power (or rate) in one of the two bands, the UE location, delay and AoD of the dominant MPC at frame t . This problem is relevant, for instance, in initial network access, where the BS can use information from control signal (e.g., over the cmWave band) to assign the suitable frequency band for data communication. It is furthermore relevant in nomadic scenarios, where the channel state does not (or not significantly) change over time, and thus even a sequential BA degenerates to the one-shot approach.

2) *Sequential Band Assignment*: In this problem, we assume that as the UE moves, the BS uses the current and the *previous* observations to predict the best band *after* U time frames. Similar to above, the used observations depend on the approach. This problem is useful for resource allocation, as the BS can plan what resources to use in advance. Note that although this problem (with small modifications) can be viewed as a generalization of the previous one, we keep the two distinct for clarity.

C. Solutions Overview

1) *Gaussian Process Based Solutions*: In this approach, assuming that the $\zeta^b(t)$ in (1) consists of path-loss $P_L^b(t)$ and large scale fading (shadowing) $S^b(t)$, i.e.,

$$\zeta^b(t) = -P_L^b(t) + S^b(t) \quad (3)$$

we assume that the BS knows the channel model and statistics, and it can estimate $P_L^b(t)$, either using empirical models or prior knowledge of the environment. Also we assume that the shadowing is a stationary Gaussian process in space (time) and frequency with mean $\mu_b = 0$ and standard deviation σ_b in band b , i.e., $S^b(t) \sim \mathcal{N}(0, \sigma_b^2)$, and $S^b(t)$ and $S^{b'}(t')$ are jointly normal with correlation function $\text{Cov}(S^b(t), S^{b'}(t'))$. An example of the correlation model and further discussion is provided in Sec. III and in [26]. Note that assuming $S^b(t)$ is Gaussian on a dB scale matches many measurement campaigns [1], but it may not always hold in practice. Still, we rely on it along with the joint Gaussian assumption over frequency for simplicity and mathematical tractability. To emphasize the fact that the rate is a random quantity, we use (3) to rewrite (1):

$$R^b(t) = \omega_b \log(1 + \gamma'_b 10^{\gamma S^b(t)}). \quad (4)$$

where $\gamma = 0.1$ and $\gamma'_b = 10^{(P_{\text{tx}}^b - P_L^b - N_0^b) \times 0.1}$. To simplify the notation we sometimes omit the time index for S^b and R^b when things are in clear context. Then, for the two problems we have

- For the one-shot problem, the BS observes $\text{SNR}^b(t)$ and uses an estimate of the path loss $P_L^b(t)$ to extract $S^b(t)$. Then it uses $S^b(t)$ to make a BA decision based on the probabilities that $R^b(t) > R^{b'}(t)$, i.e., whether to communicate over b or b' .
- For the sequential decision problem, in time frame t the BS uses the SNR observations (along with the path loss estimates) of the current and the last Q time frames to predict the BA decision in time frame $t + U$ based on the probability that $R^b(t + U) > R^{b'}(t + U)$.

For the GP-based solutions we refer to the set of observations at time t as set \mathcal{H}_t . In general, it is easy to observe that this approach uses power (rate) and distance information; it also uses training data to acquire the statistics of the environment. However, it is difficult to directly incorporate other features. Thus we consider two different environments, one of which matches the GP channel model.

2) *Learning Based Solutions:* In any given frame the BS has to take one of two decisions: use cmWave band ($\mathcal{D} = 0$) or the mmWave band ($\mathcal{D} = 1$), which can be viewed as binary classification problem. Several ML models can be used to solve such problems. Our focus will be here on NNs based solutions, but we also consider other models to provide fair assessments of the ML based solutions. The following is a summary of the used approaches:

- For the one-shot problem, we use multi-layer NNs, in addition to LR and GR. The regression models are simple linear and nonlinear ML solutions to the problem. Depending on the

environment, we could use the received power in one band, the polar coordinate of the UE (distance and phase), delay and the AoD of the dominant MPC as features.

- For the sequential problem, we use a deep network with NN and LSTM architecture. We also use a multi-layer NN and GR with historical data for comparison, the history being a window of the last Q observations. The observed features depend on the environment, but in this case they may include the observed power from both frequency bands.⁴

For the learning based solutions, we denote the set of observed features in time frame t by \mathcal{F}_t . Details of chosen approaches, training etc. are presented in Sec. IV.

D. Performance Metrics

We evaluate the performance of the solutions using the probability of BA error. For N_X number of instances it can be numerically equivalent to the average number of BA errors ⁵

$$\bar{\mathcal{E}}_X = \frac{1}{N_X} \sum_i^{N_X} |\mathcal{D}_i - \mathcal{L}_i|. \quad (5)$$

where \mathcal{D}_i and $\mathcal{L}_i \in \{0, 1\}$ are the decision of the scheme of interest and the correct decision, respectively, for instant i . We also refer to \mathcal{L}_i as the true label that takes "1" when the *data rate* in the mmWave band is larger than the data rate in the cmWave band. Note here we use *instant* i rather than time t as the data points over which we evaluate the performance may not belong to the same sequential data. We use the subscript X to distinguish the data sets for which we evaluate the BA error as we will discuss later. For interpretability of the results, we also show the normalized rate loss of the BA procedures. For *a given scheme*, we can define the achievable rate as $R_i : \{R_i^b : b = m \text{ if } \mathcal{D}_i = 1, \text{ or } b = m \text{ if } \mathcal{D}_i = 0\}$. We also define the maximum achievable rate for that instant as $R_{\max,i} = \max_{b \in \{c,m\}} R_i^b$, then the normalized rate loss is given by

$$\bar{\mathcal{R}}_X = \frac{1}{N_X} \sum_{i=1}^{N_X} \left| \frac{R_i - R_{\max,i}}{R_{\max,i}} \right| \quad (6)$$

To calculate the rate loss values, we bound the achievable rates by using a fix modulation format for both bands, in particular, we use 256 QAM. Although we will show $\bar{\mathcal{R}}_X$ alongside $\bar{\mathcal{E}}_X$ throughout this paper, we will only discuss the latter in the interpretation of the results.

⁴This is just one of many possible features, in practice this can be realized using passive power sensing (RSSI sensors) [1].

⁵Since some of the data points are correlated we rely on an argument similar to the one we gave in [26].

III. GAUSSIAN PROCESS BASED BA

Based on the model introduced in Sec. II-C1, we denote the following two events

$$\mathcal{W}_b(t) : R^b(t) > R^{b'}(t), \quad b \neq b', b, b' \in \{c, m\}.$$

Then given the set of observations at time frame t \mathcal{H}_t , a reasonable band assignment rule is

$$b^* = \arg \max_{b \in \{c, m\}} \mathbb{P}(\mathcal{W}_b(t) | \mathcal{H}_t) \quad (7)$$

This rule is a Maximum A posteriori Probability (MAP) Decision rule [28]. Next we have the following theorem.

Theorem 1. *Minimum BA error probability can be achieved when the BS chooses band b^* that satisfies*

$$b^* : \mathbb{P}(\mathcal{W}_{b^*}(t) | \mathcal{H}_t) \geq 0.5.$$

Proof. The proof is simple. We start by showing that the rule is equivalent to (7). Note that we have two cases, $\mathcal{W}_b(t)$ or $\mathcal{W}_{b'}(t)$, thus from (7) we choose b when

$$\begin{aligned} \mathbb{P}(\mathcal{W}_b(t) | \mathcal{H}_t) &\geq \mathbb{P}(\mathcal{W}_{b'}(t) | \mathcal{H}_t) \\ &\geq 1 - \mathbb{P}(\mathcal{W}_b(t) | \mathcal{H}_t), \end{aligned}$$

reordering the terms we have $\mathbb{P}(\mathcal{W}_b(t) | \mathcal{H}_t) \geq 0.5$. Next, by the definition of the MAP rule in (7), the BS minimizes the probability of error at *each* time frame, which as a result minimizes the overall probability of BA error. \square

The Theorem indicates that the natural choice for γ_T is optimal under the conditions above.

A. One-Shot Scenario

In this scenario the observation is the rate (power) in one band. Here we focus on the case when we need to decide whether to assign the UE to the mmWave band, as the other direction is safer in general and can be derived similarly. Thus we have $\mathcal{H}_t = \{S^c(t)\}$, then the rule is

$$\mathbb{P}(R^m \geq R^c | S^c = s_c) \geq 0.5. \quad (8)$$

We can rewrite the probability in (8) as:

$$\mathbb{P}\left(\omega_m \log(1 + \gamma'_m 10^{\gamma S^m}) \geq \omega_c \log(1 + \gamma'_c 10^{\gamma S^c}) \middle| S^c = s_c\right) = \mathbb{P}\left(S^m \geq v_1 \middle| S^c = s_c\right), \quad (9)$$

where $v_1 = \frac{1}{\gamma \log_{10}(\frac{1}{\gamma_m}(\exp^{r_c/\omega_m} - 1))}$, and $r_c = \omega_c \log(1 + \gamma'_c 10^{\gamma s_c})$. With the assumption that S^m and S^c are jointly normal, it is enough to determine the conditional mean $\mu_{m|c}$ and variance $\sigma_{m|c}^2$ to calculate the probability in (9), which can be shown to be

$$\mu_{m|c} = \rho_{m,c} \frac{\sigma_m}{\sigma_c} s_c \quad \text{and} \quad \sigma_{m|c}^2 = (1 - \rho_{m,c}^2) \sigma_m^2,$$

where $\rho_{m,c}$ is the correlation coefficient of S^m and S^c . Thus we have

$$\mathbb{P}(S^m \geq v_1 | S^c = s_c) = \mathbb{Q}\left(\frac{v_1 - \mu_{m|c}}{\sigma_{m|c}}\right) \geq 0.5,$$

where $\mathbb{Q}(\cdot)$ is the Q-function [29]. Taking the inverse of Q-function, and rearranging the terms, we have

$$v_1 \leq \mathbb{Q}^{-1}(0.5) \sigma_{m|c} + \mu_{m|c} = \rho_{m,c} \frac{\sigma_m}{\sigma_c} s_c,$$

where we have used the fact that $\mathbb{Q}^{-1}(0.5) = 0$. Solving for s_c , the BS should assign the UE to the mmWave band if the following condition is satisfied:

$$S^c \geq \frac{\sigma_c}{\rho_{m,c} \sigma_m} v_1. \quad (10)$$

For consistency with [27], we refer to this scheme as Threshold Based BA (TBBA).

B. Sequential BA

1) *Exact Solution*: The sequential BA follows similar steps, however, we here have $\mathcal{H}_t = \{S^c(t-Q), S^c(t-Q+1), \dots, S^c(t), S^m(t-Q), S^m(t-Q+1), \dots, S^m(t)\}$. The goal is to choose either $\mathcal{W}_c(t+U)$ or $\mathcal{W}_m(t+U)$. Thus we choose $b^* = m$ if:

$$\mathbb{P}(\mathcal{W}_m(t+U) | \mathcal{H}_t) \geq 0.5 \quad (11)$$

and $b^* = c$ otherwise. Since the set \mathcal{H}_t has more than a single value, we need to use the joint Gaussian assumption over time (space). Then (11) becomes

$$\begin{aligned} \mathbb{P}(\mathcal{W}_m(t+U) | \mathcal{H}_t) &= \mathbb{P}(R^m(t+U) \geq R^c(t+U) | \mathcal{H}_t) \\ &= \int_{-\infty}^{\infty} \mathbb{P}(R^m(t+U) \geq R^c(t+U) | \mathcal{H}_t, S^c(t+U) = s) f_{S^c | \mathcal{H}_t}(s) ds. \end{aligned} \quad (12)$$

where $f_{S^c | \mathcal{H}_t}(s)$ is the probability density function (PDF) of $S^c(t+U)$ given \mathcal{H}_t , which follows a normal distribution with mean $\mu_{c|H}$ and variance $\sigma_{c|H}^2$. Note that we conditioned on $S^c(t+U)$ and used the integration to circumvent the fact that the probability of $\mathcal{W}^m : \{R^m > R^c\} =$

$\{R^m - R^c > 0\}$ cannot be calculated using a simple probability distribution without some crude approximations (as we discuss in the next subsection). Next, using (4) we rewrite (12) as:

$$\int_{-\infty}^{\infty} \mathbb{P}(S^m(t+U) \geq \mathcal{V}_2(s) | \mathcal{H}_t, S^c(t+U) = s) f_{S^c | \mathcal{H}_t}(s) ds, \quad (13)$$

where $\mathcal{V}_2(s) = \frac{1}{\gamma} \log_{10} \left(\frac{1}{\gamma'_m} \left(\exp \left(\frac{\omega_c}{\omega_m} \log(1 + \gamma'_c 10^{\gamma s}) \right) - 1 \right) \right)$

In order to evaluate (13), we first point out that $S^m(t+U)$, $S^c(t+U)$ and the observations in \mathcal{H}_t are jointly normal, thus it is enough to calculate the conditional mean and variance of $S^m(t+U)$ given \mathcal{H}_t and $S^c(t+U)$, which we denote by $\mu_{m|H^+}$ and $\sigma_{m|H^+}^2$, respectively. Note that we refer to the set of $\{S^c(t+U) \cup \mathcal{H}_t\}$ by \mathcal{H}_t^+ . To calculate these quantities we need to define a few vectors and matrices: we use the convention that $\Sigma_{\mathcal{X}}$ denotes the covariance matrix between the elements of a set of random variables \mathcal{X} . We also denote $\Sigma_{\mathcal{X},y}$ as the cross covariance vector between \mathcal{X} and a random variable Y , and $\Sigma_{y|\mathcal{X}}$ is the variance of Y given a realization of elements of \mathcal{X} . For instance, Σ_H is a $(Q+1) \times (Q+1)$ covariance matrix of the shadowing observations, $\Sigma_{H,b}$ is a $(Q+1) \times 1$ vector that represents the covariance between the shadowing in band b at time $t+U$ and data in set \mathcal{H}_t . We use a similar subscript convention for the means, where $\mathbf{m}_{\mathcal{X}}$ refers to the vector of individual mean values of \mathcal{X} , and $\mu_{y|\mathcal{X}}$ refers to the mean of Y given \mathcal{X} . Then it is easy to verify that [29]:

$$\mu_{m|H^+} = \mu_m + \Sigma_{m,H^+} \Sigma_{H^+}^{-1} (\mathbf{k} - \mathbf{m}_{H^+}) = \Sigma_{m,H^+} \Sigma_{H^+}^{-1} \mathbf{k}, \quad (14)$$

where $\mathbf{k} = [s, \text{vec}(\mathcal{H}_t)^\top]^\top$, where $\text{vec}(\mathcal{X})$ converts the set \mathcal{X} to a vector. Also we have

$$\sigma_{m|H^+}^2 = \sigma_m^2 - \Sigma_{m,H^+} \Sigma_{H^+}^{-1} \Sigma_{m,H^+}^\top. \quad (15)$$

Similarly, for $S^c(t+U)$ given \mathcal{H}_t , we have:

$$\begin{aligned} \mu_{c|H} &= \mu_c + \Sigma_{c,H} \Sigma_H^{-1} (\mathbf{h} - \mathbf{m}_H) = \Sigma_{c,H} \Sigma_H^{-1} \mathbf{h} \\ \sigma_{c|H} &= \sigma_c^2 - \Sigma_{c,H} \Sigma_H^{-1} \Sigma_{c,H}^\top, \end{aligned}$$

where $\mathbf{h} = \text{vec}(\mathcal{H}_t)$. Note that as indicated earlier, to calculate these quantities, we have to know the correlation model as well as the path-loss values.

2) *Approximation:* We can provide a simpler rule that does not rely on integration by assuming that $w_b \log(1 + 10^{\text{SNR}^b(t)}) \approx w_b \log(10^{\text{SNR}^b(t)})$, which is usually referred to as the "high SNR assumption". Then we have:

$$\tilde{R}^b = \omega_b \log(\gamma_b) + \frac{\log(10)}{10} \omega_b S^b,$$

which follows a normal distribution with mean and variance, respectively:

$$\tilde{\mu}_b = \omega_b \log(\gamma_b), \quad \text{and} \quad \tilde{\sigma}_b^2 = \left(\frac{\log(10)}{10} \right)^2 \omega_b^2 \sigma_b^2.$$

Then we can define the event $\tilde{\mathcal{W}}_b(t+U) : \tilde{R}^b(t+U) \geq \tilde{R}^{b'}(t+U)$, and choose b that satisfies $\mathbb{P}(\tilde{\mathcal{W}}_b|\mathcal{H}_t) > 0.5$. To calculate this probability, and taking $b = m$ and $b' = c$, we have:

$$\mathbb{P}(\tilde{\mathcal{W}}_m|\mathcal{H}_t) = \mathbb{P}(\tilde{R}_m(t+U) - \tilde{R}^c(t+U) \geq 0|\mathcal{H}_t) = \mathbb{P}(\tilde{R}_D \geq 0|\mathcal{H}_t),$$

where $\tilde{R}_D = \tilde{R}^m(t+U) - \tilde{R}^c(t+U)$, since S^m and S^c are jointly normal, so is \tilde{R}^m and \tilde{R}^c , and thus \tilde{R}_D is normally distributed with mean and variance, respectively:

$$\mu_D = \tilde{\mu}_m - \tilde{\mu}_c \quad \text{and} \quad \sigma_D^2 = \tilde{\sigma}_m^2 + \tilde{\sigma}_c^2 - 2\rho_{m,c}\tilde{\sigma}_m\tilde{\sigma}_c.$$

Furthermore, note that \tilde{R}_D given \mathcal{H}_t is normally distributed, with mean and variance, respectively:

$$\begin{aligned} \mu_{D|H} &= \mu_D + \Sigma_{D,H}\Sigma_H^{-1}\mathbf{h}, \quad \text{and} \\ \sigma_{D|H} &= \sigma_D^2 - \Sigma_{D,H}\Sigma_H^{-1}\Sigma_{D,H}^\top. \end{aligned}$$

Finally, the decision rule becomes $\mathbb{Q}\left(\frac{-\mu_{D|H}}{\sigma_{D|H}}\right) \geq 0.5$, which can be shown to be equivalent to

$$\mu_{D|H} \geq 0 \implies \tilde{\mu}_c - \tilde{\mu}_m \leq \Sigma_{D,H}\Sigma_H^{-1}\mathbf{h} \quad (16)$$

Due to the simplicity of this rule one can easily derive a number of interesting quantities, such as the probability of error, however, we omit such discussion due to space limitations. We hereafter refer to the exact and approximate GP based solutions, respectively, as GP and GP_{App}. In Sec. V we study the impact of the decision threshold γ_T and observation window Q on both solutions.

IV. LEARNING BASED BAND ASSIGNMENT

A. Preliminaries

As introduced in Sec. II-C2, the BS uses the input features \mathcal{F} to the ML to produce $\tilde{\mathcal{D}}$ and then that to make the BA decision \mathcal{D} . The BS can use a threshold $\gamma_T \in [0, 1]$ to map $\tilde{\mathcal{D}}$ to \mathcal{D} , where we assume that $\mathcal{D} = 1$ when $\tilde{\mathcal{D}} > \gamma_T$. We can choose γ_T that results in the best performance, however, we here do that only for the one-shot problem, and use $\gamma_T = 0.5$ for the sequential problem.

1) *Features*: We consider six features, i.e., side information that are used as input to the learning solutions: (f_1) the distance from the BS to the UE d in meters, (f_2) the angular position of the UE θ in rad, (f_3) the received signal strength (or the SNR) in the cmWave band in dBm (or dB), (f_4) similar quantities in the mmWave band, (f_5) the delay of the dominant MPC in seconds, and (f_6) the AoD of the dominant MPC, where the dominant MPC is the one with the highest power.

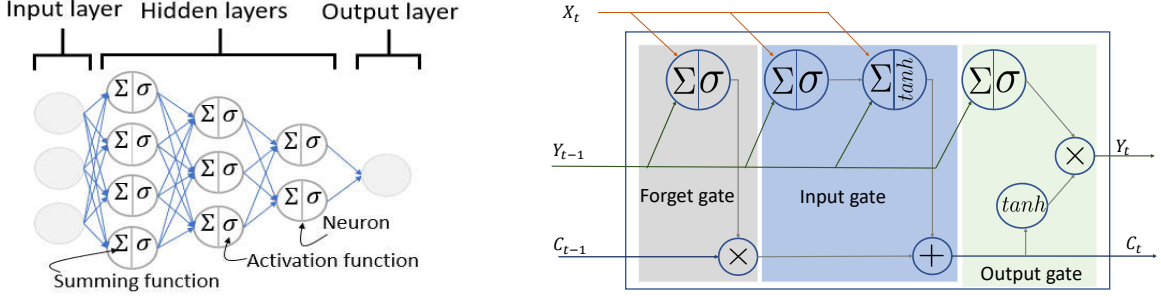
The availability of the features depends on the system implementations. For instance, (f_1) and (f_2), i.e., (d, θ) (which represent the polar coordinates of the UE with respect to the BS), may be estimated using signal processing techniques or acquired by explicit feedback of the GPS data. To extract (f_5) large bandwidth might be required, for (f_6) the use of antenna arrays is necessary. Using both (f_3) and (f_4) is only reasonable for the sequential BA problem, but it may require additional effort or equipment at the UE side. We consider several combinations of the above features and discuss their effectiveness for BA.

As typically done in ML, we perform pre-processing of the features, in particular we standardize the input features such that their mean is zero and the standard deviation is equal to one. In addition, we utilize the prior knowledge about the wireless propagation, for instance we use logarithmic scale for distances and power, as this may linearize their relation with one another.

2) *Learning Techniques Overview*: LR (Linear regression) is a simple ML approach, where the output is assumed to be a linear combination of the input features. Although the linear models are relatively simple, they have been widely used in wireless communication [1]. Since the BA can be viewed as a binary classification, GR (logistic regression) can better fit to our problem, where the linear combinations of the features are mapped by a logistic function to the range $[0, 1]$, thus representing the probability of the output being in one of the classes. NNs (artificial neural networks) have been successfully applied to many complex practical problems. An NN consists of one or more layers, each of which has a number of parallel neurons (nodes), see Fig. 1a. The neuron performs a weighted combination of the input features and then passes it through a possibly non-linear transformation, also known as an activation function, e.g., a sigmoid function (generalization of the logistic function). Note that the GR can be viewed as a simple NN that consists of one neuron.

LSTM (Long Short Term Memory) is a popular Recurrent NN architecture. The inputs of the LSTM are the current features, the previous output and the previous cell state. The cell state is a memory that is controlled by three gates, which control when to read, to write and to erase

the value of the cell. The decisions of the gates are controlled by NNs that provide nonlinear transformations of the input values, Fig. 1b shows a diagram of an LSTM layer. The weights of the above solutions are determined during the training phase over a training dataset \mathcal{A}^T , where the goal is to minimize the prediction error of the label values at the output over the observed data points. Popular training techniques use gradient descent, such as backpropagation for NNs and backpropagation through time for LSTM.



(a) Illustration of a neural network with two hidden layers.

(b) Long Short Term Memory (LSTM).

Fig. 1: NN and LSTM diagrams.

3) *Training and Testing:* To train the learning approaches, we assume that the BS uses a data set $\mathcal{A}^T = \{\mathcal{P}_1^T, \dots, \mathcal{P}_{N_T}^T\}$, where the *superscript* T denotes training, and N_T is the number of training examples. Each example point \mathcal{P}_i^T is a features-label pair $(\mathcal{F}_i, \mathcal{L}_i)$, where \mathcal{F}_i is the set of features of the i th example of size $F = |\mathcal{F}_i|$, $|\cdot|$ denoting the cardinality operator. As in Sec. II-D, $\mathcal{L}_i \in \{0, 1\}$ is the true label of that example. We assume that \mathcal{A}^T is available to the BS, for instance through previous decisions or an initial network training phase. However, the procedure to acquire \mathcal{A}^T is out of the scope of the paper.

In this work, let the set \mathcal{A} denotes the entire data set we use in each environment, where each point $\mathcal{P}_i \in \mathcal{A}$ represents the features label pair $(\mathcal{F}_i, \mathcal{L}_i)$, where $i \in \{1, \dots, N\}$ and $N = |\mathcal{A}|$. In the simulation we *randomly* split \mathcal{A} into a training set \mathcal{A}^T and a testing set \mathcal{A}^S , where $\mathcal{A} = \mathcal{A}^T \cup \mathcal{A}^S$ and $\mathcal{A}^T \cap \mathcal{A}^S = \emptyset$. We may further split \mathcal{A}^T into a training subset \mathcal{A}_t^T and a validation subset \mathcal{A}_v^T , $\mathcal{A}_t^T \cap \mathcal{A}_v^T = \emptyset$. The sizes of $\mathcal{A}_t^T, \mathcal{A}_v^T$ and \mathcal{A}^S are respectively N_T, N_V , and N_S . More details about this are provided in the next sections. During the *training phase*, as it is commonly used in binary classification problems, the performance of the learning approaches is evaluated using a Cross Entropy (CE) cost function, i.e.,

$$\bar{\mathcal{E}}_{\text{CE},X} = \frac{1}{N_X} \sum_i^{N_X} (-\mathcal{L}_i \log(\tilde{\mathcal{D}}_i) - (1 - \mathcal{L}_i) \log(1 - \tilde{\mathcal{D}}_i)).$$

As in Sec. II-D, we use the subscript X to distinguish the used data set to calculate these value. For the introduced data sets we have $X \in \{T, V, S\}$.

B. One-Shot BA

In this problem we use LR, GR and NN learning approaches. For NN we use up to four hidden layers and up to 100 neurons in total. We use L2 regularization to reduce the impact of over-fitting with parameter α . For each time instant, the input feature size for each of the approaches is equal to the number of used features. For this problem we use Monte-Carlo cross validation to improve our estimate of the validation error, in which we repeat the random split of \mathcal{A}^T to \mathcal{A}_t^T and \mathcal{A}_v^T , and rerun the training and the validation. Then we choose the network structure (number of layers and neurons in the NN) and regularization coefficient α that achieve the smallest *average* $\bar{\mathcal{E}}_{\text{CE},V}$. To choose the hard decision threshold γ_T we use the value in $[0, 1]$ that results on the smallest *average* $\bar{\mathcal{E}}_V$. Finally note that we use similar training, cross validation and method to obtain the hard decisions for LR and GR as well.

C. Sequential BA

In this problem we use previously observed data points to predict the best band after U future time frames. We use a DL approach based on LSTM and also use GR-based (denoted by GR_H), and NN-based (denoted by NN_H) approaches for comparison. We consider several DL structures, they are summarized in the Table I. For each features scenario we choose the network that results in the lowest cross validation error, we refer to this approach as LSTM_{opd} . In Secs. V and VI we show the performance of LSTM_{opd} and NW4, we refer to the latter as LSTM_{std} . We use the *Adam* algorithm for training [30]. The number of used epochs depends on whether we shuffle the data set at the beginning of each iteration, we use up to 600 epochs when we shuffle the data set, and up to 120 when we do not, for the former case the size of the minimum batch is three sequences (to be explained later) while it is four for the latter case. We use an initial learning rate of 0.01 and a drop factor of 0.1 and 0.009 when we shuffle and do not shuffle respectively, the learning rate drops after 120 and 50 epochs for the two cases respectively. The choice between the two is done based on the cross validation. For NN_H we use two hidden layers with 70 and 40 neurons, respectively.

Since the decision depends on the previous data points, we use a modified dataset $A^{T'}$. In particular, the labels at point (time) i are $\mathcal{L}'_i = \mathcal{L}_{i+U}$. In addition, to utilize the Q previous

Network	Structure (Layer: Size)	Network	Structure (Layer: Size)
NW0	(FC: 5)+(LSTM: 5)+(FC: 5)	NW8	(FC: $3 \times F$)+(LSTM: $3 \times F$)+(FC: $2 \times F$)
NW1	(FC: 15)+(LSTM: 10)+(FC: 10)	NW9	(FC: $10 \times F$)+(LSTM: $9 \times F$)+(FC: $5 \times F$)
NW2	(FC: 50)+(LSTM: 10)+(FC: 10)	NW10	(FC: $10 \times F$)+(LSTM: $5 \times F$)
NW3	(FC: 30)+(LSTM: 20)+(FC: 15)	NW11	(FC: $5 \times F$)+(LSTM: $10 \times F$)
NW4	(FC: 20)+(LSTM: 40)+(FC: 20)	NW12	(LSTM: $10 \times F$)
NW5	(FC: 15)+(LSTM: 10)+(FC: 10)+(ReLU)+(FC:7)	NW13	(FC: $3 \times F$)+(LSTM: $15 \times F$)+(FC: $4 \times F$)
NW6	(FC: 10)+(LSTM: 50)+(FC: 7)	NW14	(FC: 20)+(LSTM: 40)+(ReLU)
NW7	(FC: $2 \times F$)+(LSTM: $2 \times F$)+(FC: $2 \times F$)	NW15	(FC: $3 \times F$)+(LSTM: $15 \times F$)+(FC: $4 \times F$)+(ReLU)

TABLE I: DL structures, note that all structures are followed by (FC:2)+(SOFT)+(CLASS), where FC is a fully connected linear transformation layer (parallel neurons), ReLU: a nonlinear ReLU layer [9], SOFT: a softmax layer, CLASS: classification layer, F is the features size. The hidden size of the LSTM layer is shown after "LSTM".

observed points in the GR_H and NN_H , their data sets should have input features size $|\mathcal{F}'| = F \times (Q + 1)$, i.e., the size is equal to the number of used features in the current and the Q previous points. For the DL approach, no modification to the feature size is needed, because the LSTM layer has a memory and can select what to remember and what to forget. Note that in this manuscript we focus on $|\mathcal{L}'_i| = 1$ for simplicity. We consider the other case in our future work, where we can use sequence-to-sequence learning based on LSTM encoder/decoder [31].

Due to the size of the problem, we use fixed γ_T and α values. In particular we use the "natural" choice $\gamma_T = 0.5$ as we will discussed in the next section.

V. EXPERIMENT I: STOCHASTIC ENVIRONMENT

Here we study the performance of the solutions using stochastically generated channels. This will provide a comparison between the learning based and the GP based solutions in a synthetic environment that matches the GP assumptions. We first describe the general data generation model and then address the dataset details and the performance for each of the two problems. In this section and the one follows, due to the space limit, we only discuss the main results, however, the tables and figures contain more information and are left for the reader's reference. Note that for the learning schemes, we emphasize that the displayed performance values are by no means the optimal values, as we have considered a limited number of structures and parameters and performed a grid search over them.

A. The Environment

In order to generate the channel realizations in the two bands, we use a modified correlation model of the one suggested in [26]. The covarinace between shadowing values at time instants t and t' and in frequency bands b and b' is

$$\text{Cov}\left(S^b(t), S^{b'}(t')\right) = \rho_{b,b'} \sqrt{\mathbf{C}\left(S^b(t), S^b(t')\right) \mathbf{C}\left(S^{b'}(t), S^{b'}(t')\right)}, \quad (17)$$

where $\rho_{b,b'}$ is the correlation coefficients, and

$$\mathbf{C}\left(S^b(t), S^b(t')\right) = \exp\left(-\left(\frac{\Delta(t,t')}{d_{\text{dcor}}^b}\right)^\nu\right) \sigma_b^2, \quad (18)$$

where $\Delta(t, t')$ is the displacement (in meters) between the location of the UE at times t and t' , d_{dcor}^b is the shadowing decorrelation distance in band b (in meters), the real coefficient $\nu > 0$ is a decay exponent [32], values for ν in $(0, 2]$ have been previously used [32]. Note that with $\nu = 1$ (18) is equivalent to the popular Gudmundson correlation model [33]; with this value, we observed that the schemes show small dependency on prior observations, which may not reflect practical environments, thus we consider two values of ν in the sequential problem. We assume that the path-loss follows a break point path-loss model [1], with a break distance d_{break} and a propagation exponent 2 for $d \leq d_{\text{break}}$ and ϵ for $d > d_{\text{break}}$. Table II summarizes the values used for generating the data sets.

Variable	Band c/m
f_b	2.5/28 GHz
Bandwidth ω_b	10/100 MHz
P_{tx}^b	15/22 dBm
ϵ	4
d_{break}	50 m
d_{dcor}	25/24
σ_b	5/7 dB
$\rho_{m,c}$	0.75
ν	{1, 1.9}
Noise Spectral Density	-174 dBm/Hz

Variable	Band c/m
f_b	2.5/28 GHz
Ant. Pattern	Isotropic
Ant. Polarization	Vertical
P_{tx}^b	15/30 dBm
BS height	45 m
MS height	2 m
Max. Diffraction	2/1
Max. Reflection	10

TABLE II: Stochastic channel simulation configurations **TABLE III:** Ray-tracing simulation configurations.

B. One-Shot BA

1) *Data Points:* We assume that the BS is located at the center of a square cell with a side length of 500 m, the data set consists of 2000 data points, which correspond to 2000 uniformly distributed UEs around the BS. We choose $\nu = 1.9$.⁶ In this data set, to simplify the simulation environment, we focus on three features: location of the UE (d, θ) and the power in the cmWave band. We here use 65% of the data set for training. For the Monte-Carlo cross validation, we take around 20% of \mathcal{A}^T for the validation subset \mathcal{A}_v^T . We generate 1000 independent cell realizations to assess the performance of the learning based BA and the TBBA in the stochastic environment.

⁶Note that this is different from [27], however, the results that we discuss below are consistent with [27] due to the fact that the value of ν has small impact on the one-shot problem.

Feature / Combination	c-1	c-2	c-3	c-4	c-5	c-6	c-7
d	✓	✓		✓	✓		
θ	✓	✓	✓				✓
cmWave Power		✓	✓	✓		✓	
NN $\bar{\mathcal{E}}_S$.24	.186	.189	.194	.267	.195	.413
NN $\bar{\mathcal{R}}_S$.099	.067	.068	.071	.115	.071	.223
GR $\bar{\mathcal{E}}_S$.265	.191	.192	.192	.266	.193	.469
GR $\bar{\mathcal{R}}_S$.115	.07	.07	.07	.115	.071	.261
LR $\bar{\mathcal{E}}_S$.264	.195	.193	.195	.265	.194	.469
LR $\bar{\mathcal{R}}_S$.113	.072	.07	.072	.114	.071	.261
TBBA $\bar{\mathcal{E}}_S$.193			
TBBA $\bar{\mathcal{R}}_S$.07			

TABLE IV: Performance of the learning over the stochastic data under different feature availability. Note that on average 49.3% of the labels are "1".

2) *Performance:* We can view each of the 1000 cell realizations as a different cell. Then for every realization we repeat the training, validation and then testing. Table IV summarizes the results for seven feature combinations. The last row shows the performance of the TBBA (GP based). In the generated data set we have about 50.7% of the labels are "0". Thus, assigning the cmWave band, i.e., cmWave-only BA, for all points would result in error equal 0.493.

In general, we notice the learning techniques provide significant improvements over the cmWave-only BA, with an advantage to the NN over the other schemes, as the NN is able to learn the non-linearity in the feature(s)/BA mapping. This can be observed in the performance for the first features combination (c-1), i.e., the location of the UE. Next, adding the received power in the cmWave band, (c-2), provides an evident performance gain for all learning approaches. In fact, it seems that any other combination with the power information would provide comparable performance, especially when we use the angle information as in (c-3).

Comparing power-only (c-6) to distance-only (c-5), we observe that the power in the cmWave band seems to reveal more information about the BA than the distance. In fact, we notice that the performance in (c-4) is close to (c-6). This should not be surprising, as the shadowing is better captured with the received power in the cmWave band compared to the distance. However, we notice an improvement in (c-3) compared to (c-4), as the angle will provide additional information that helps to identify clusters of similar BA decisions.

For the TBBA, from the table we notice that the learning schemes can be at least as good as the TBBA in several features combinations. These results have been achieved without providing the structure and the statistics of the channels. In fact, the NN is able to outperform the TBBA in (c-2) and (c-3). Note that with only power feature, the learning based solutions are roughly as good as the TBBA. Further discussion can be found in [27].

C. Sequential BA

1) *UE Trajectories*: In this problem the data set consists of *sequences* of features and labels that represent different UE trajectories and the optimal BA decisions; each sequence can be viewed as an ordered subset of the available data points. Generation of such a data set is challenging, as we have to generate correlated data points and reasonable trajectories. Note that the points on different trajectories may still be correlated as they belong to the same realization of the environment. As a result, we restrict our environment to one realization with several trajectories, we further generate the trajectories over a grid that represents the cell.

We use a Semi Markov Smooth mobility model (SMS) to generate the motion trajectories [34]. In a SMS model, the UE motion goes through cycles of four states until the end of the simulation time; it starts with the acceleration state with a random direction and a maximum ultimate speed, then a steady motion state, next it decelerates to zero before it stops in the last state, the UE can then go again to the first state. The duration of each state is a design parameter, we assume that the duration of the second state is a random value whose minimum is equal to half of the simulation time, during this state it maintains the speed and the direction with a high probability. In our simulation, we omit the repeated data points (the consecutive points on the trajectories that correspond to the same location), and limit the number of repeated crossings over the same grid point. This model captures two important aspects of the realistic pedestrians mobility, the smooth speed and direction adaptation (during the second state), and the possibility of changing the direction and speed along the route (at the beginning of the first state).

2) *Data Generation*: We use the same network structure (cell dimension, path loss model, frequency and bandwidths) as above with 5 m separation distance between the points on the grid. We generated 1000 sequences, we assumed that the duration for each sequence is 900 s with speed up to 1.5m/s and a 4 s sampling period. To generate the shadowing values we use the correlation model in (17) for two different ν values, $\nu = 1$ and $\nu = 1.9$. We assume that the observation window of GP-based and learning-based solutions (other than LSTM-based) is five, i.e., $Q = 5$. For training we use 70% of the sequences for training and 30% for testing. For the LSTM based solution we use 50 sequences for cross validation. To assess the power of the solutions we consider the prediction over two different future values $U = 4$ and $U = 8$.

3) *Performance ($\nu = 1$)*: The results are presented in Table V. As before the first five rows show the features combinations, then for each solution we show the BA error $\bar{\mathcal{E}}_S$ in the first row

Feature / Combination	c-1	c-2	c-3	c-4	c-5	c-6	c-7
d	✓	✓		✓	✓		
θ	✓		✓	✓	✓		
cmWave Power		✓	✓	✓	✓	✓	✓
mmWave Power					✓	✓	
LSTM _{opd} $\bar{\mathcal{E}}_S$.178/.198	.195/.214	.183/.238	.164/.196	.159/.193	.192/.244	.206/.248
LSTM _{opd} $\bar{\mathcal{R}}_S$.068/.077	.081/.088	.073/.1	.062/.078	.062/.078	.077/.102	.083/.103
LSTM _{std} $\bar{\mathcal{E}}_S$.178/.198	.193/.214	.183/.233	.165/.192	.163/.192	.191/.243	.206/.252
LSTM _{std} $\bar{\mathcal{R}}_S$.068/.077	.078/.088	.073/.099	.064/.076	.065/.077	.079/.107	.083/.104
NN _H $\bar{\mathcal{E}}_S$.211/.216	.216/.227	.197/.244	.192/.214	.189/.207	.209/.251	.22/.257
NN _H $\bar{\mathcal{R}}_S$.08/.082	.083/.087	.074/.101	.072/.082	.071/.08	.081/.104	.085/.106
GR _H $\bar{\mathcal{E}}_S$.22/.225	.22/.229	.214/.25	.209/.225	.198/.227	.211/.257	.221/.256
GR _H $\bar{\mathcal{R}}_S$.085/.088	.083/.089	.082/.103	.079/.088	.074/.088	.081/.107	.086/.106
GP $\bar{\mathcal{E}}_S$.201/.226			
GP $\bar{\mathcal{R}}_S$.075/.088			
GP _{App} $\bar{\mathcal{E}}_S$.221/.242			
GP _{App} $\bar{\mathcal{R}}_S$.082/.095			

TABLE V: Sequential BA $\nu = 1$: Performance of the learning over the stochastic data under different feature availability. Note that on average 47.9% of the labels are "1". The first number in each entry in rows 6 – 17 denotes the prediction error with $U = 4$, and the second with $U = 8$.

and the normalized rate loss $\bar{\mathcal{R}}_S$ in the second row for the two U values (separated by "/"). Starting with $U = 4$, we notice that GP_{App} shows around 9% degradation in the performance compared to GP. For learning schemes we notice that all-features combination (c-5) provides the best performance followed by the combination of cmWave power and location (c-4). One reason for (c-5)'s good performance seems to be the location information. This conjecture is supported by the performance of (c-1) compared to having cmWave and mmWave powers (c-6). The importance of location information is intuitive, as it relates to trajectory prediction which in turn impacts the channel conditions. The performance difference between the LSTM-based solutions and NN_H may be attributed to the inherent ability of LSTM layer for sequential learning. Note that the cmWave and mmWave power combination (c-6) still provides valuable information, and with it as the basis, most of the learning schemes outperform GP, and all of them outperform GP_{App}. This is important as both approaches, the GP-based and the ML-based, may use cmWave and mmWave power as input observations. Interestingly, we also observe that using a cmWave only (c-7) learning scheme can outperform GP_{App}.

For $U = 8$, we first notice that the performance degradation of GP_{App} compared to GP reduces to about 7%. We also observe that the learning schemes can still outperform the GP-based solution, especially using (c-5) and (c-4), however, the number of combinations and schemes that outperform GP-based solution reduces, and the gain that the best learning solution provides (LSTM_{opd} using (c-5)) reduces from 21% to 15%. Using power(s) only to solve the problem becomes less efficient, as it is clear in the case of (c-6), where only the LSTM-based scheme

can compete with GP_{App} . This is expected as the learnability for large U is harder, Fig. 2 emphasizes this trend for combinations (c-5) and (c-6) as function of U . The figure also shows that $LSTM_{std}$ dominates the other schemes for small U , but the probability of BA error increases logarithmically as U increases.

From the table, for most of the combinations, we observe that $LSTM_{std}$ shows relatively good performance, this might be attributed to its medium size as smaller and larger networks are more susceptible to fitting problems. Note that for some cases, the table shows that $LSTM_{std}$ has slightly better performance than $LSTM_{opd}$, despite the fact that the schemes included in $LSTM_{opd}$ cover $LSTM_{std}$, this is attributed to the small cross validation set.

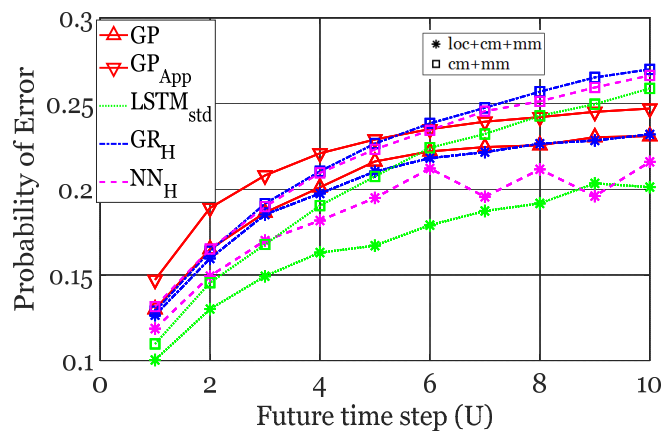


Fig. 2: $\bar{\mathcal{E}}_S$ vs. U for two combination "loc+cm+mm" and "cm+mm" ((c-6) and (c-5), respectively, in Table V).

The use of $\gamma_T = 0.5$ for GP was justified in Sec. III, in Fig. 3 we present the impact of γ_T on the performance for combinations (c-5) and (c-6), and show the performance for the $LSTM_{std}$ (as listed in the table) for comparison. We notice that $\gamma_T \approx 0.5$ is good for most of the schemes except GP_{App} , indicating that GP_{App} can be improved with a judicious choice of γ_T .

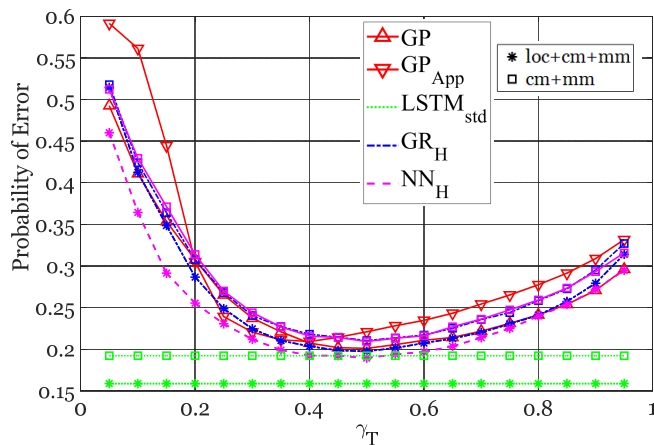


Fig. 3: $\bar{\mathcal{E}}_S$ vs. the decision threshold γ_T with for $\nu = 1$ for two features combinations "loc+cm+mm" and "cm+mm", respectively, (c-5) and (c-6) in Table V.

Feature / Combination	c-1	c-2	c-3	c-4	c-5	c-6	c-7
d	✓	✓		✓	✓		
θ	✓		✓	✓	✓		
cmWave Power		✓	✓	✓	✓	✓	✓
mmWave Power					✓	✓	
LSTM _{opd} $\bar{\mathcal{E}}_S$.166/.209	.158/.204	.139/.203	.124/.184	.103/.178	.119/.215	.166/.23
LSTM _{opzd} $\bar{\mathcal{R}}_S$.068/.089	.06/.084	.052/.087	.046/.075	.034/.074	.042/.096	.063/.097
LSTM _{std} $\bar{\mathcal{E}}_S$.166/.204	.158/.206	.142/.203	.123/.185	.107/.175	.119/.215	.166/.229
LSTM _{std} $\bar{\mathcal{R}}_S$.068/.085	.062/.085	.053/.087	.045/.077	.037/.074	.042/.096	.063/.099
NN _H $\bar{\mathcal{E}}_S$.196/.209	.18/.211	.155/.217	.147/.201	.118/.195	.136/.231	.176/.233
NN _H $\bar{\mathcal{R}}_S$.077/.085	.067/.084	.055/.091	.051/.081	.036/.077	.042/.098	.066/.099
GR _H $\bar{\mathcal{E}}_S$.21/.215	.18/.211	.169/.228	.172/.207	.127/.206	.133/.229	.179/.232
GR _H $\bar{\mathcal{R}}_S$.085/.087	.067/.084	.063/.097	.064/.082	.038/.081	.04/.096	.067/.099
GP $\bar{\mathcal{E}}_S$.126/.204			
GP $\bar{\mathcal{R}}_S$.037/.08			
GP _{App} $\bar{\mathcal{E}}_S$.159/.225			
GP _{App} $\bar{\mathcal{R}}_S$.052/.089			

TABLE VI: Sequential BA $\nu = 1.9$: Performance of the learning over the stochastic data under different feature availability. Note that on average 48.4% of the labels are "1".

4) *Performance* ($\nu = 1.9$): With $\nu = 1.9$, the correlation function decays faster than above, however, we noticed that the impact of prior observations is more pronounced. The results for several features observations are presented in Table VI with a structure similar to the one above. For $U = 4$, we first observe that GP outperforms GP_{App} by about 20%, and several learning schemes outperform the GP with several features combinations. In addition, the all-features combination (c-5) still has the least $\bar{\mathcal{E}}_S$, but different than above the performance gain is attributed to the power in the two bands (c-6). Interestingly, LSTM-based solutions using cmWave power feature (c-7) is as good as location (comparable to GP_{App}) in this environment, which indicates that (c-7) is a good BA predictor. The significance of (c-7) is also evident for other learning schemes that use an observation window.

For $U = 8$, we notice a similar trend as in $\nu = 1$, namely that the values of $\bar{\mathcal{E}}_S$ increase, the gain of GP over GP_{App} reduces to about 9%, and the gain of the best learning combination/scheme, (c-5)/ LSTM_{opd}, reduces from 18.3% to 12.8%. However, these gains are larger than in $\nu = 1$, due to the utilization of the observations. Compared to $U = 4$ the efficacy of observed powers reduces, for instance (c-1) outperforms (c-6) and (c-7); this is due to the fact the shadowing decorrelates with large separation distances. Nevertheless, the LSTM-based schemes are able to utilize the cmWave power when accompanied with other features, in (c-2), (c-3) and (c-4), and shows at least comparable performance to GP.

Based on the used pedestrians speed, grid points separation and sampling interval we anticipate that observations outside the used observation window, of size $Q = 5$, have small influence on the BA at time frame $t + U$. However, considering the adopted motion model, this may not be

accurate, as an old observation might be highly correlated (closely located) to future value. This complicates the analysis of the impact of Q . Instead we here restrict our attention to a simpler motion model, namely a circular motion around the BS, where we consider 5000 sequences, each corresponding to one circle around the BS and having an independent shadowing realization; we here relax some of the correlation assumption since we consider only cmWave and mmWave power information. The results are provided in Fig. 4. The learning schemes achieve the same performance compared to the *optimal* solution (GP in this case). Starting with GP vs. GP_{App} , it is clear that the approximation introduces an error floor for GP_{App} . The GP_{App} shows a noticeable decrease in $\bar{\mathcal{E}}_S$ until $Q = 4$, as it may reduce the uncertainty, however beyond that the error increases again due to the model mismatch. While an increase of Q improves the performance for GP and the learning schemes, we notice a slower improvement for large Q , due to the decrease of added information in older observations in such a uniform motion. A more comprehensive study is needed for this problem but it highly depends on the motion model.

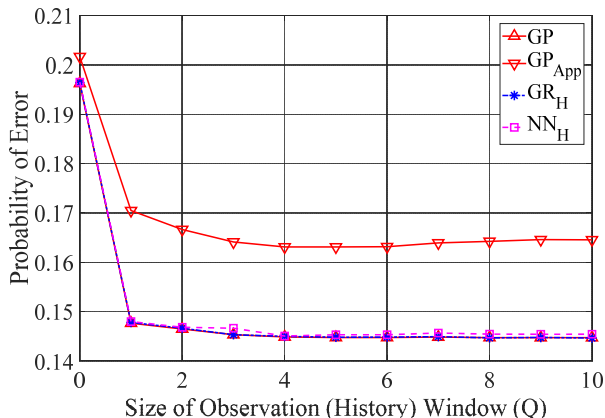


Fig. 4: The impact of the size of the observation window Q in stochastic environment with circular trajectory. For this data set the percentage of "1"s is 75%.

VI. EXPERIMENT II: SIMULATED CAMPUS ENVIRONMENT

A. The Environment

To assess the performance in a more realistic setting, we simulate the propagation channel in a campus environment by means of a commercial ray-tracing tool, Wireless InSite [35]. The input to the ray-tracer includes the 3D models of the buildings, the characteristics of the building materials and models of foliage. The output is a list of parameter vectors that contains the power, propagation delay, the AoD and AoA, for each MPC. Simulation results have been compared to measurements in a variety of settings and shown to provide good agreement [35]. This simulation has been conducted based on the model of the University Park Campus, University of Southern

California, which is shown in Fig. 5-(a). The detailed simulation configurations are listed in Table III. The simulation environment was also used in prior works, see references in [27].

The data set has about 1150 points, i.e., $|\mathcal{A}| = 1150$, each point contains all the six features. The label that is associated with each point is whether the rate in the mmWave band is larger than the one in the cmWave band. To calculate the rate we use the Shannon capacity with bandwidth and noise spectral density that are shown in Table II.

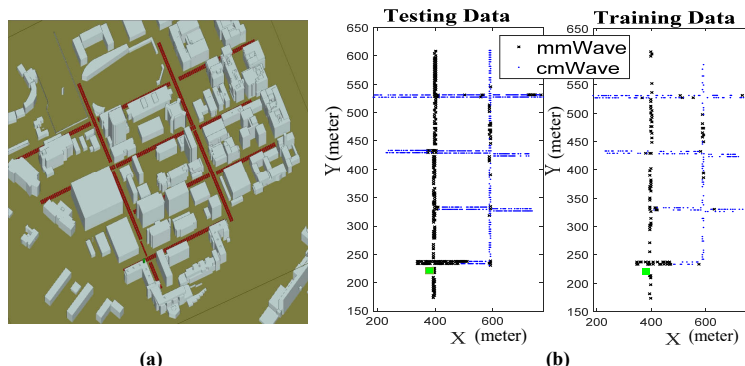


Fig. 5: (a) Ray-tracing simulation environment. The green dot is the BS located above the rooftop, while simulated UEs are red routes. Gray objects represent the buildings. The green 3D polygons denote foliage with different densities. (b) Using 70% of the data for testing, from left to right \mathcal{A}^S and \mathcal{A}^T .

B. One-Shot

1) *Data Points:* Since acquiring a large number of data points may not be practical for the BS, using a large portion of the data set for training may produce misleading results. Here we use only 30% of \mathcal{A} for training. To apply the Monte-Carlo cross-validation method, we randomly choose 80% of \mathcal{A}^T for training and 20% for validation. The network is then tested on \mathcal{A}^S , i.e., the remaining 70% of the data set. Fig. 5-(b) shows an example of the sets \mathcal{A}^S and \mathcal{A}^T .

Feature /Combination	c-1	c-2	c-3	c-4	c-5	c-6	c-7	c-8
d	✓	✓	✓			✓		
θ	✓	✓						
cmWave Power		✓	✓	✓	✓		✓	
Delay				✓			✓	✓
AoD							✓	✓
Numb Layers/ α/γ_T	2/.15/.45	4/.15/.55	1/.05/.5	1/.1/.6	2/.1/.35	3/.5/.45	4/.3/.6	3/.5/.55
NN $\bar{\mathcal{E}}_S$.078	.061	.072	.074	.085	.182	.067	.093
NN $\bar{\mathcal{R}}_S$.05	.032	.041	.042	.054	.133	.037	.062
GR $\bar{\mathcal{E}}_S$.178	.062	.082	.081	.083	.183	.082	.182
GR $\bar{\mathcal{R}}_S$.129	.032	.051	.049	.051	.135	.048	.13
LR $\bar{\mathcal{E}}_S$.176	.078	.088	.078	.081	.178	.072	.188
LR $\bar{\mathcal{R}}_S$.126	.047	.054	.047	.049	.128	.04	.136

TABLE VII: Performance of the learning techniques on ray-tracing data, under different feature availability, note that the percentage of points with labels equal to "1" is approximately 30%.

2) *Performance:* We first point out that in this environment using cmWave-only BA would result in an error equal to 0.3, i.e., the percentage of "1" in \mathcal{A} is 30%. Table-VII summarizes the

results of the solutions. The used structures of the NNs are shown in the 7th row. Combinations (c-1) and (c-8) show the cases when we use the location or the delay and AoD of the strongest MPC; these two are usually related as several localization techniques use the delay and AoD to determine the location. The performance in the two cases are comparable, even though we may not have Line of Sight (LOS) in all the cases. We also note that NN significantly outperforms the regression-based approaches.

Adding the power to the two combinations above, as in (c-2) and (c-7), improves the performance for this environment as well, especially for the regression-based BA. The performance gain in (c-2) and (c-7) can be partially explained by the good results in (c-5) that uses the cmWave power only. As in the stochastic environment, a scheme that only exploits the distance feature (c-6) shows relatively poor performance for all approaches. Similar comparisons can be made with a delay-only (not shown in the table) scheme, which provides an improvement compared to distance only [27]. This performance could be expected as that the delay may reflect a more realistic effective distance, note that non-LOS links will show a longer delay even if they have similar geographic distance as their LOS counterpart. A combination of delay and distance with power, in (c-3) and (c-4), shows small improvement over power only, however, they show significant improvement over distance-only and delay-only cases. In general, we notice that in this environment, the performance gaps between NN and other learning based solutions are larger than for the stochastic environment, which suggests that in a more realistic environment, the NN is especially useful.

C. Sequential BA

1) *Data Points*: To generate the sequences we use the motion model discussed in Sec. V-C1 over the ray-tracing grid. This includes the pedestrians speed, simulation time, and sampling interval. We generate 1000 sequences, and use 350 of them for training out of which 70 are chosen randomly for cross validation for the LSTM-based solution. In this problem we apply the GP-based solutions; to do so we extract the channel parameters to fit the path-loss (using a double linear fit) and then compute the parameter for the correlation model (17) and (18).

2) *Performance*: Table VIII shows the performance of the schemes in this environment with a structure similar to the ones in Sec. V-C. We start by observing that both GP-based solutions are not performing well This can be explained by our investigation of the shadowing distribution in this environment, where we observed that it is far from satisfying the GP assumption even

Feat./Comb.	c-1	c-2	c-3	c-4	c-5	c-6	c-7	c-8	c-9	c-10	c-11
d	✓	✓	✓								
θ	✓	✓	✓							✓	
cmWave		✓	✓	✓	✓			✓	✓	✓	✓
mmWave			✓	✓		✓			✓		
Delay							✓	✓	✓		✓
AoD							✓	✓	✓		
LSTM _{opd} $\bar{\mathcal{E}}_S$.078/.117	.062/.103	.062/.1	.07/.12	.094/.14	.08/.132	.098/.137	.071/.114	.061/.11	.071/.12	.081/.128
LSTM _{opd} $\bar{\mathcal{R}}_S$.048/.08	.044/.074	.041/.071	.048/.085	.061/.1	.062/.092	.065/.098	.048/.08	.046/.078	.048/.086	.054/.089
LSTM _{std} $\bar{\mathcal{E}}_S$.077/.117	.064/.108	.062/.1	.07/.123	.094/.14	.08/.132	.096/.134	.073/.118	.065/.111	.071/.12	.079/.126
LSTM _{std} $\bar{\mathcal{R}}_S$.048/.081	.044/.075	.042/.071	.048/.089	.062/.1	.053/.094	.067/.096	.049/.086	.044/.08	.047/.086	.053/.09
NN _H $\bar{\mathcal{E}}_S$.086/.11	.083/.119	.076/.116	.107/.139	.134/.162	.12/.15	.113/.147	.098/.117	.085/.117	.099/.144	.107/.152
NN _H $\bar{\mathcal{R}}_S$.053/.073	.052/.081	.047/.078	.068/.096	.088/.114	.078/.103	.074/.105	.063/.082	.054/.081	.063/.103	.068/.106
GR _H $\bar{\mathcal{E}}_S$.208/.211	.134/.156	.123/.15	.125/.156	.142/.17	.122/.153	.224/.231	.138/.166	.119/.155	.137/.164	.14/.168
GR _H $\bar{\mathcal{R}}_S$.149/.151	.089/.11	.08/.104	.081/.108	.096/.121	.079/.106	.16/.166	.092/.117	.078/.108	.091/.116	.093/.106
GP $\bar{\mathcal{E}}_S$.183/.177										
GP $\bar{\mathcal{R}}_S$.127/.123										
GP _{App} $\bar{\mathcal{E}}_S$.159/.174										
GP _{App} $\bar{\mathcal{R}}_S$.107/.119										

TABLE VIII: Performance of the solutions on ray-tracing data under different feature availability. The percentage of points with labels equal to "1" is approximately 30%. Results in rows 8-19 correspond to $U = 4/U = 8$.

for a single band. We also note that the GP has a larger $\bar{\mathcal{E}}_S$ compared to GP_{App} (14% worse for $U = 4$); this surprising result might be related to the fact that GP is only exact if the Gaussian model is fulfilled, so that an approximate algorithm might suffer less in the presence of model mismatch. For the learning schemes we focus on the performance of LSTM-based and NN_H. For $U = 4$, we notice that the location plus the powers in both bands (c-3) still achieves low $\bar{\mathcal{E}}_S$, however, note that for LSTM-based solutions this is the case for other combination as well such as the powers in both bands plus AoD and Delay (c-9). Comparing $\bar{\mathcal{E}}_S$ for the power in both bands (c-4), location (c-1), and AoD and Delay (c-7), we notice that (c-4) plays a major role in the performance gain that we observed. The value that (c-4) achieve is also possible using other combinations, namely (c-8) and (c-10), which require the cmWave power plus other features, indicating the practicality of the solutions when only the cmWave power (e.g., through a control signal) is periodically observed. Note that, for LSTM-based scheme, $\bar{\mathcal{E}}_S$ for (c-1) is not much worse than (c-4), which explains why the *combination* of location and cmWave power (c-2) would be as good as (c-3). For NN_H things are slightly different as the observed performance gain is mainly attributed to the location information (c-1), which alone provides a performance comparable to (c-9).

For $U = 8$, we observe that (c-3) is the best features combination for LSTM_{opd}, while location only (c-1) is the best for NN_H; the performance gain for LSTM_{opd} over NN_H (using their best features combinations) reduces from 19.7% to 9.1%; this could be explained by the observed degradation of the efficacy of (c-4) compared to (c-1), as the correlation of the shadowing

reduces, and the fact that NN_H can utilize the location information well. Combining location or Delay and AoD with other features provides just a slight advantage for the LSTM_{opd} , however, for other combinations the LSTM_{opd} outperforms NN_H significantly, possibly due to the fact that these features combination are less relevant to location information. Note that the observed behaviour of the LSTM based solutions and NN_H with the location information and the power of both bands was also observed in stochastic environment with $\nu = 1.9$.

The impact of U is further shown in Fig. 6. The probabilities of error $\bar{\mathcal{E}}_S$ using (c-3) and (c-9) are comparable over different U , which is interesting as this could eliminate the need for explicit feedback of the location information. For the GP based scheme, as discussed above, GP_{App} is better than GP. One reason for the relative better performance can be attributed to the intuitive GP_{App} structure, eq. (16), which is a threshold rule that employs the gap between the average received powers in the two bands, which may rely less on the impact of the GP assumption on the rates. Note that the general behaviour of the GP-based solution can be explained by the fact that the environment does not follow the GP assumption anymore, but rigorous explanations are difficult since we here have a single environment realization.

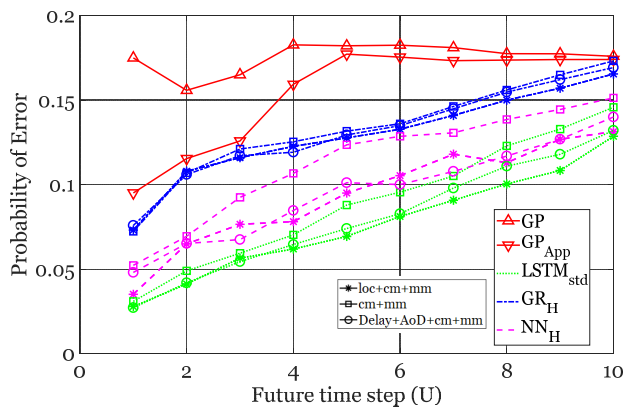


Fig. 6: $\bar{\mathcal{E}}_S$ vs. U for three features combinations "loc+cm+mm", "cm+mm" and "Delay+AoD+cm+mm", respectively, (c-3), (c-4) and (c-9) in Table VIII.

VII. CONCLUSION

In this paper, we explored learning-based and GP-based approaches to provide solutions to the BA problem in two scenarios; (i) one-shot BA and (ii) sequential BA. We considered two environments to assess the performance of the proposed techniques and gain insights about the impact of different features, using stochastic and ray-tracing simulations. We also discussed the impact of prediction horizon and the observation window.

The performance depends on the problem and the used features. For the one-shot problem, the learning based approaches showed competitive performance to the GP-based solution, especially

when the SNR in one band is known. For the sequential BA, the DL scheme (LSTM based) showed superior performance due to its inherent ability to deal with sequential data. NN-based and LSTM-based solutions using location and power information in the two bands have consistently shown to be the best BA decision predictor; however, LSTM-based solutions using other information including delay and AoD also showed competitive performance. Interestingly, in realistic environments, the power information has proven to be especially beneficial for short prediction horizon. We also observed that the GP-based solutions have failed in the ray-tracing environment. In general, the LSTM and NN based solutions show good performance using features that are relatively easy to acquire, indicating the practicality of the learning solutions.

REFERENCES

- [1] A. F. Molisch, *Wireless Communications*. IEEE Press - Wiley; 2 edition, 2011.
- [2] A. Ali, N. González-Prelcic, and R. W. Heath, “Estimating millimeter wave channels using out-of-band measurements,” in *Info. Theory and App. Works, (ITA), 2016*. IEEE, 2016, pp. 1–6.
- [3] J. G. a. Andrews *et al.*, “What will 5G be?” *IEEE Jour. on select. areas in comm.*, vol. 32, no. 6, pp. 1065–1082, 2014.
- [4] N. González-Prelcic *et al.*, “Millimeter-wave communication with out-of-band information,” *IEEE Comm. Mag.*, vol. 55, no. 12, pp. 140–146, 2017.
- [5] K. Chandra, R. V. Prasad, B. Quang, and I. Niemegeers, “CogCell: cognitive interplay between 60 GHz picocells and 2.4/5 GHz hotspots in the 5G era,” *IEEE Communications Magazine*, vol. 53, no. 7, pp. 118–125, 2015.
- [6] S.-Y. Lien *et al.*, “5G new radio: Waveform, frame structure, multiple access, and initial access,” *IEEE communications magazine*, vol. 55, no. 6, pp. 64–71, 2017.
- [7] S. Sangodoyin, U. Virk, D. Burghal, A. Molisch, and K. Haneda, “Joint characterization of mm-wave and cm-wave device-to-device MIMO channels,” in *Military Communications Conference, MILCOM 2018-2018 IEEE*, 10 2018.
- [8] M. Chen *et al.*, “Machine learning for wireless networks with artificial intelligence: A tutorial on neural networks,” *arXiv preprint arXiv:1710.02913*, 2017.
- [9] T. OShea and J. Hoydis, “An introduction to deep learning for the physical layer,” *IEEE Trans. on Cogn. Comm. and Net.*, vol. 3, no. 4, pp. 563–575, 2017.
- [10] T. Wang *et al.*, “Deep learning for wireless physical layer: Opportunities and challenges,” *China Comm.*, vol. 14, no. 11, pp. 92–111, 2017.
- [11] T. J. a. O’Shea *et al.*, “Deep learning based MIMO communications,” *arXiv preprint arXiv:1707.07980*, 2017.
- [12] N. Farsad and A. Goldsmith, “Neural network detection of data sequences in communication systems,” *arXiv preprint arXiv:1802.02046*, 2018.
- [13] T. Nitsche *et al.*, “Steering with eyes closed: Mm-wave beam steering without in-band measurement,” in *2015 IEEE Conf. on Comp. Comm. (INFOCOM)*, April 2015, pp. 2416–2424.
- [14] M. Hashemi *et al.*, “Out-of-band millimeter wave beamforming and communications to achieve low latency and high energy efficiency in 5G systems,” *IEEE Trans. on Comm.*, 2017.
- [15] A. Ali, N. González-Prelcic, and R. W. Heath Jr, “Spatial covariance estimation for millimeter wave hybrid systems using out-of-band information,” *arXiv preprint arXiv:1804.11204*, 2018.

- [16] O. Semiari, W. Saad, and M. Bennis, "Joint millimeter wave and microwave resources allocation in cellular networks with dual-mode base stations," *IEEE Trans. on Wirel. Comm.*, 2017.
- [17] H. Chergui, K. Tourki, R. Lguensat, M. Benjillali, C. Verikoukis, and M. Debbah, "Classification algorithms for semi-blind uplink/downlink decoupling in sub-6 GHz/mmwave 5G networks," *arXiv preprint arXiv:1809.01583*, 2018.
- [18] F. B. Mismar and B. L. Evans, "Partially blind handovers for mmwave new radio aided by sub-6 GHz LTE signaling," in *Proc. IEEE Int. Conf. on Communications Work. Evolutional Tech. & Ecosystems for 5G Phase II*, 2018.
- [19] A. Alkhateeb and I. Beltagy, "Machine learning for reliable mmwave systems: Blockage prediction and proactive handoff," *arXiv preprint arXiv:1807.02723*, 2018.
- [20] J. Riihijarvi and P. Mahonen, "Machine learning for performance prediction in mobile cellular networks," *IEEE Computational Intelligence Magazine*, vol. 13, no. 1, pp. 51–60, 2018.
- [21] Y. Wang, M. Martonosi, and L.-S. Peh, "Predicting link quality using supervised learning in wireless sensor networks," *ACM SIGMOBILE Mobile Computing and Communications Review*, vol. 11, no. 3, pp. 71–83, 2007.
- [22] J. Wang *et al.*, "Spatiotemporal modeling and prediction in cellular networks: A big data enabled deep learning approach," in *INFOCOM 2017-IEEE Conference on Computer Communications, IEEE*. IEEE, 2017, pp. 1–9.
- [23] L. S. Muppirisetty, T. Svensson, and H. Wymeersch, "Spatial wireless channel prediction under location uncertainty," *IEEE Trans. on Wireless Comm.*, vol. 15, no. 2, pp. 1031–1044, 2016.
- [24] S. Chen, Z. Jiang, J. Liu, R. Vannithamby, S. Zhou, Z. Niu, and Y. Wu, "Remote channel inference for beamforming in ultra-dense hyper-cellular network," in *GLOBECOM 2017-2017 IEEE Global Comm. Conf.* IEEE, 2017, pp. 1–6.
- [25] S. Navabi, C. Wang, O. Y. Bursalioglu, and H. Papadopoulos, "Predicting wireless channel features using neural networks," in *Comm. (ICC), 2016 IEEE Int Conf. on*. IEEE, 2018, pp. 1–6.
- [26] D. Burghal and A. F. Molisch, "Rate and outage probability in dual band systems with prediction-based band switching," *IEEE Wireless Communications Letters*, pp. 1–1, 2018.
- [27] D. Burghal, R. Wang, and A. F. Molisch, "Band assignment in dual band systems: A learning-based approach," *arXiv preprint arXiv:1810.01534 [eess.SP]*, 2018.
- [28] S. M. Kay, "Fundamentals of statistical signal processing, vol. ii: Detection theory," *Signal Processing. Upper Saddle River, NJ: Prentice Hall*, 1998.
- [29] A. Leon Garcia, *Probability, statistics, and random processes for electrical engineering*. Pearson Education; 3rd ed., 2008.
- [30] D. P. Kingma and J. Ba, "Adam: A method for stochastic optimization," *arXiv preprint arXiv:1412.6980*, 2014.
- [31] I. Sutskever, O. Vinyals, and Q. V. Le, "Sequence to sequence learning with neural networks," in *Advances in neural information processing systems*, 2014, pp. 3104–3112.
- [32] S. S. Szyszkowicz *et al.*, "On the feasibility of wireless shadowing correlation models," *IEEE Trans. on Veh.r Tech.*, vol. 59, no. 9, pp. 4222–4236, 2010.
- [33] M. Gudmundson, "Correlation model for shadow fading in mobile radio systems," *Electronics letters*, vol. 27, no. 23, pp. 2145–2146, 1991.
- [34] M. Zhao and W. Wang, "WSN03-4: A Novel Semi-Markov Smooth Mobility Model for Mobile Ad Hoc Networks," in *Global Telecommunications Conference, 2006. GLOBECOM'06. IEEE*. IEEE, 2006, pp. 1–5.
- [35] W. I. Remcom, "https://www.remcom.com/wireless-insite-em-propagation-softwareinsite-wireless-em-propagation-more-info," online, accessed: March 2017.